

# Design and fabrication of Si-HDPE hybrid Fresnel lenses for infrared imaging systems

AHMAD ROSLI ABDUL MANAF,<sup>1,2</sup> TSUNETOSHI SUGIYAMA,<sup>3</sup> AND JIWANG YAN<sup>1,\*</sup>

<sup>1</sup>Department of Mechanical Engineering, Keio University, Yokohama 223-8522, Japan

<sup>2</sup>Faculty of Manufacturing Engineering, Universiti Malaysia Pahang, 26600 Pekan, Pahang, Malaysia

<sup>3</sup>Light for Wave Corporation, Saitama 350-0313, Japan

\*yan@mech.keio.ac.jp

**Abstract:** In this work, novel hybrid Fresnel lenses for infrared (IR) optical applications were designed and fabricated. The Fresnel structures were replicated from an ultraprecision diamond-turned aluminum mold to an extremely thin layer (tens of microns) of high-density polyethylene polymer, which was directly bonded onto a flat single-crystal silicon wafer by press molding without using adhesives. Night mode imaging results showed that the fabricated lenses were able to visualize objects in dark fields with acceptable image quality. The capability of the lenses for thermography imaging was also demonstrated. This research provides a cost-effective method for fabricating ultrathin IR optical components.

© 2017 Optical Society of America

**OCIS codes:** (220.3620) Lens system design; (220.4000) Microstructure fabrication; (220.4610) Optical fabrication; (110.3080) Infrared imaging.

## References and links

1. N. A. Kulakova, A. R. Nasyrov, and I. M. Nesmelova, "Current trends in creating optical systems for the IR region," *J. Opt. Technol.* **77**(5), 324–330 (2010).
2. T. Grulois, G. Druart, H. Sauer, M. Chambon, N. Guérineau, S. Magli, G. Lasfargues, and P. Chavel, "Reduction of material mass of optical component in cryogenic camera by using high-order Fresnel lens on a thin germanium substrate," *Appl. Opt.* **54**(20), 6313–6320 (2015).
3. T. Grulois, G. Druart, N. Guérineau, A. Crastes, H. Sauer, and P. Chavel, "Extra-thin infrared camera for low-cost surveillance applications," *Opt. Lett.* **39**(11), 3169–3172 (2014).
4. J. Yan, M. Yoshino, T. Kuriyagawa, T. Shirakashi, K. Syoji, and R. Komanduri, "On the ductile machining of silicon for micro electro-mechanical systems (MEMS), opto-electronic and optical applications," *Mater. Sci. Eng. A* **297**(1-2), 230–234 (2001).
5. J. Yan, K. Maekawa, J. Tamaki, and T. Kuriyagawa, "Micro grooving on single-crystal germanium for infrared Fresnel lenses," *J. Micromech. Microeng.* **15**(10), 1925–1931 (2005).
6. J. Yan, K. Syoji, and J. Tamaki, "Some observations on the wear of diamond tools in ultra-precision cutting of single-crystal silicon," *Wear* **255**(7-12), 1380–1387 (2003).
7. R. N. Claytor, N. E. Claytor, W. M. Drive, and F. Worth, "Low-cost polymer infrared imaging lens," *Proc. SPIE* **5074**, 855–866 (2003).
8. D. Vicker and R. LeBlanc, "Midwave infrared imager with plastic laminated diffractive / aspheric surfaces," *Proc. SPIE* **4369**, 642–648 (2001).
9. D. Vicker, "Molded and laminated infrared imager Laminated Kino / Asphere," *SPIE* **5074**, 814–817 (2003).
10. A. R. Abdul Manaf and J. Yan, "Press molding of a Si-HDPE hybrid lens substrate and evaluation of its infrared optical properties," *Precis. Eng.* **43**, 429–438 (2016).
11. M. Worgull, M. Schneider, M. Heilig, A. Kolew, H. Dingreiter, and J. Mohr, "Replication of optical components by hot embossing," *SPIE* **7716**, 771604 (2010).
12. L. Peng, Y. Deng, P. Yi, and X. Lai, "Micro hot embossing of thermoplastic polymers: a review," *J. Micromech. Microeng.* **24**(1), 013001 (2014).
13. J. Yan, T. Zhou, N. Yoshihara, and T. Kuriyagawa, "Shape transferability and microscopic deformation of molding dies in aspherical glass lens molding press," *J. Manuf. Technol. Res.* **1**, 85–102 (2009).
14. T. Zhou, J. Yan, J. Masuda, T. Oowada, and T. Kuriyagawa, "Investigation on shape transferability in ultraprecision glass molding press for microgrooves," *Precis. Eng.* **35**(2), 214–220 (2011).
15. A. Nikonorov, R. Skidanov, V. Fursov, M. Petrov, S. Bibikov, and Y. Yuzifovich, "Fresnel lens imaging with post-capture image processing," in *IEEE Comput. Soc. Conf. Comput. Vis. Pattern Recognit. Work.* (2015), pp. 33–41.
16. J. W. Horwitz, "Infrared refractive index of polyethylene and a polyethylene-based material," *Opt. Eng.* **50**(9), 93603 (2011).

#280748

<http://dx.doi.org/10.1364/OE.25.001202>

Journal © 2017

Received 14 Nov 2016; revised 15 Dec 2016; accepted 15 Dec 2016; published 17 Jan 2017

17. L. Li, P. He, F. Wang, K. Georgiadis, O. Dambon, F. Klocke, and A. Y. Yi, "A hybrid polymer–glass achromatic microlens array fabricated by compression molding," *J. Opt.* **13**(5), 55407 (2011).
18. A. R. Abdul Manaf and J. Yan, "Improvement of form accuracy and surface integrity of Si-HDPE hybrid microlens arrays in press molding," *Precis. Eng.* **47**, 469–479 (2017).
19. Y. He, J.-Z. Fu, and Z.-C. Chen, "Optimization of control parameters in micro hot embossing," *Microsyst. Technol.* **14**(3), 325–329 (2007).
20. C. Liu, J. M. Li, J. S. Liu, and L. D. Wang, "Deformation behavior of solid polymer during hot embossing process," *Microelectron. Eng.* **87**(2), 200–207 (2010).
21. X. Zhu, T. W. Simon, and T. Cui, "Hot embossing at viscous state to enhance filling process for complex polymer structures," *Microsyst. Technol.* **18**(3), 257–265 (2011).
22. T. Fujii, A. Goulet, K. Hattori, K. Konno, A. Tanaka, R. Bosmans, M. Sawada, and H. Yazawa, "Fresnel lens sidewall design for imaging optics," *J. Eur. Opt. Soc.* **10**, 15017 (2015).

## 1. Introduction

Infrared (IR) imaging systems are widely used in various applications such as rescue, night surveillance, night driving assistance, as well as thermography. The reduction of the size and production cost of an IR lens play a significant role in the mass production of compact IR imaging systems. Therefore, the demand for developing new high-precision IR lens fabrication techniques is rapidly rising.

To date, several IR lens materials have been widely used, with each material having different characteristics. Germanium (Ge), for example, possesses excellent transmittance rates in the mid-to-far IR region. However, it is bulky, heavy, and expensive [1]. Silicon (Si) is relatively lower in cost compared with Ge and also lighter. However, the IR absorbance is higher than Ge. Machining Ge into a thin Fresnel shape enables the reduction of the lens weight [2]. In the Fresnel lens design, the lens curvature (concave or convex) collapses into a series of concentric narrow rings (Fresnel zone) and is flattened. Thus, it retains the optical characteristics of a normal plano-concave or plano-convex lens. The Fresnel structure is also beneficial to Si as it will result in a tolerable level of IR absorbance [3]. However, machining both Ge and Si materials is difficult and expensive due to their hard and brittle nature [4–6]. Ultraprecision machines and extremely sharpened diamond tools are necessary to enable ductile machining of Si and Ge. Additionally, the tool wear rate in diamond turning of Si is very high, leading to high production costs and degraded machining accuracy.

In recent years, the use of polymers such as high-density polyethylene (HDPE) polymer as an IR lens material has been reported, which offers a cheaper solution [7]. However, compared with Ge and Si, HDPE suffers from high IR absorbance and needs to be formed in very small thickness to obtain acceptable levels of IR transmittance. Previous researchers used a layer (~320 micron-thick) of polymer to laminate a plano-convex shaped silicon lens with adhesive and cut Fresnel structures on the polymer by diamond turning [8,9]. In a previous study, the present authors proposed an ultrathin Si-HDPE hybrid substrate for IR micro lens arrays by attaching an extremely thin (~80 micron-thick) HDPE film onto a thin and flat Si wafer without adhesives through press molding, and improved its IR transmittance [10].

In this research, we will attempt designing and directing press molding of ultraprecision Fresnel structures onto an extremely thin polymer layer of a Si-HDPE hybrid substrate to fabricate ultrathin IR night vision lenses. Press molding is an effective process for forming microstructures and high aspect ratio optical components of glass and polymers [11–14], by which high precision Fresnel lenses could be obtained at a low cost without subsequent time-consuming diamond turning process. When press molding an ultrathin Fresnel lens, it is essential to precisely control the molding conditions for improving the form accuracy and image quality of the pressed lenses. The press molding conditions should also be optimized to realize the crosslink binding between the polymer and the Si wafer substrate [10].

This paper presents the results of the design and fabrication of an ultrathin Si-HDPE hybrid Fresnel lens for night vision imaging systems. As the use of single Fresnel lens in imaging is not suitable as it suffers chromatic aberration [15], a novel double lens system,

which comprises a spherical and an aspherical plano-convex shaped Fresnel lens, was adopted to minimize the chromatic aberration. The influence of different press molding parameters on form accuracy of the resulting lens was investigated. In addition, an IR imaging trial was performed using a home-built optical system to demonstrate the optical performance of the fabricated lens system. The results of the fabricated lenses were also compared with the simulated results to verify their optical functions. To further improve the image quality, a combination of Si-HDPE hybrid Fresnel lens and a Ge lens was attempted and excellent imaging quality was realized.

## 2. Experimental procedures

### 2.1 Refractive index determination

The materials used in this research were a combination of Si and HDPE. A two-side polished Si wafer with a thickness of 755  $\mu\text{m}$  was cut into 15  $\times$  15 mm squares, while the thickness of HDPE laminating one side of the Si was 80  $\mu\text{m}$ , making the total thickness of the hybrid substrate equals 835  $\mu\text{m}$ . The thickness of HDPE needed to be maintained as thin as possible to reduce IR absorbance. A few property data of both materials were also presented in the authors' previous research [10].

Refractive index is an important factor in lens design. The refractive index of Si was obtained from the Zemax software library. However, no refractive index data can be found for HDPE from the software library. Thus, in this study, the HDPE refractive index was referred from [16]. For comparison, a Conrady fitting tool was used to calculate the refractive index ( $n$ ) of HDPE for the wavelength region of 8-13  $\mu\text{m}$ , as follows:

$$n = n_0 + \frac{a}{\lambda + b} / (\lambda^{3.5}) \quad (1)$$

where  $n_0 = 1.20048915$ ,  $a = 4.52708247$ ,  $b = -387.18421$ , and  $\lambda$  is the wavelength. These default dispersion data were obtained from Zemax software. The results of the calculated refractive index of HDPE for different wavelengths are illustrated in Fig. 1. A good fitting between the reference and calculated data was confirmed. The refractive index data was then entered into the Zemax software for lens design and analysis.

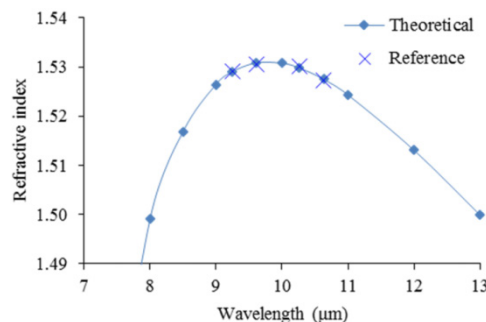


Fig. 1. Refractive index of HDPE for different IR wavelengths.

### 2.2 Hybrid lens design

A double lens system, which consists of a spherical and an aspherical plano-convex Fresnel lens, was designed using a Si-HDPE hybrid substrate. The maximum total angle of view of the lens is 30°. The first lens (Lens 1) was set to have a spherical shape with the lens curvature radius of 11.636 mm. Meanwhile, the second lens (Lens 2) of an aspherical shape was set to have a radius of 11.034 mm. Both lenses with the Fresnel structure diameter of 13.5 mm were formed on an 80  $\mu\text{m}$  thick HDPE layer of the Si-HDPE hybrid substrate. The

Si-HDPE hybrid micro Fresnel lens structure design is shown schematically in Fig. 2(a), and its parameters summarized in Table 1.

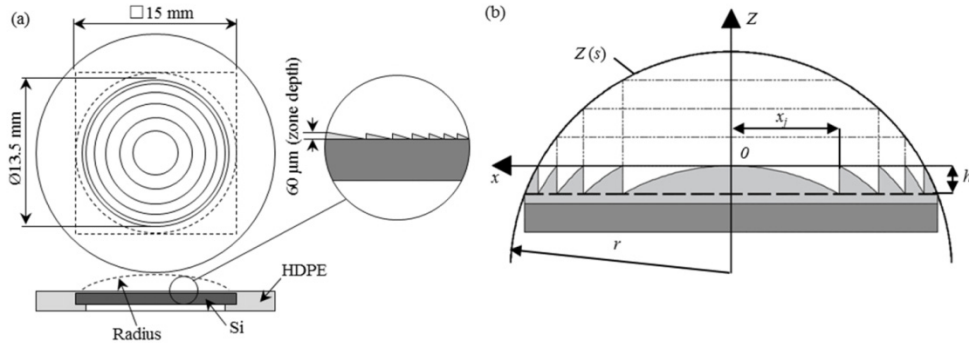


Fig. 2. Schematic diagrams of (a) Si-HDPE hybrid Fresnel lens design and (b) Fresnel structure surface geometry.

Table 1. Double Si-HDPE hybrid lens design parameters.

Parameters	Value
Lens radius ( $R$ ):	
Lens 1 (Spherical) (mm)	11.636
Lens 2 (Aspherical) (mm)	11.034
Lens 2 conic constant ( $k$ )	-2.813
Lens diameter ( $D$ ) (mm)	13.5
Fresnel zone depth ( $h$ ) ( $\mu\text{m}$ )	60
HDPE thickness ( $\mu\text{m}$ )	80
Si thickness ( $\mu\text{m}$ )	755

A thin lens maker's formula, Eq. (2), was used to calculate the focal distance ( $f$ ) of the lens.

$$\frac{1}{f} = (n_{lens} - 1) \left( \frac{1}{r} \right) \quad (2)$$

where  $n_{lens}$  represents the refractive index of the lens material, and  $r$  is the radius curvature of the lens. The refractive index of the lens material will vary for different wavelengths [17]. The wavelengths selected were between 8.5 to 12  $\mu\text{m}$  of IR region due to the accuracy of the fitted data. Meanwhile, the focal length ( $f_T$ ) of the combined lens can be calculated using the following equation, Eq. (3):

$$f_T = \left( \frac{f_1 \cdot f_2}{f_1 + f_2 - d} \right) \quad (3)$$

where  $f_1$  is the focal length of Lens 1,  $f_2$  is a focal length of Lens 2, and  $d$  is the distance between the two lenses. The combined focal length calculated by the Zemax software was 10.982 mm.

Figure 2(b) shows schematically the geometry of the surface of the Fresnel lens. The even aspherical lens curvature can be calculated using the aspheric lens equation, Eq. (4), to define the profile, as follows:

$$Z(s) = \frac{C_s^2}{1 + \sqrt{1 - (1+k)C_s^2 s^2}} + A_4 s^4 + A_6 s^6 + A_8 s^8 \quad (4)$$

where  $Z$  is sag of the surface parallel to  $Z$  axis,  $s$  is a radial distance from the optical axis,  $C$  is lens curvature (inverse of radius),  $k$  is the conic constant, and  $A_4$ ,  $A_6$ ,  $A_8$  were the order of

aspheric terms. In this study,  $A_4$ ,  $A_6$ ,  $A_8$  were set to zero, and the conic constant ( $k$ ) for the aspherical Fresnel lens of Lens 2 was set to  $-2.813$ .

The lens surface was divided into concentric rings by cylindrical surfaces at the zone steps. The radial coordinate ( $x_j$ ) of each ring can be calculated using the following equation, Eq. (5):

$$x_j = \sqrt{j \cdot h \left( \frac{2}{c} - j \cdot h \right)} \quad (5)$$

where  $j$  is the sequential number of the Fresnel zone counted from the center of the lens axis ( $z$ ) and  $h$  is the zone depth. In this case,  $h$  was set to  $60 \mu\text{m}$ . Meanwhile, to prevent light reflection at the Fresnel zone side wall, no draft angle was designed.

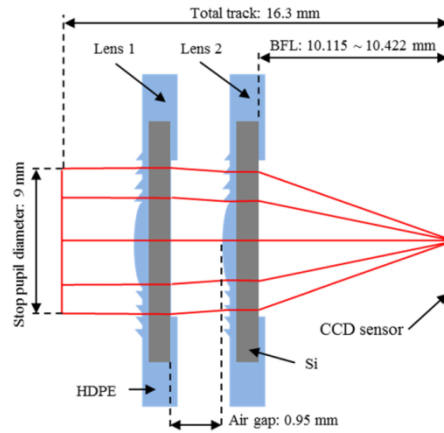


Fig. 3. Schematic diagram of a double Si-HDPE hybrid Fresnel lens system.

After obtaining the lens parameters, these parameters were entered into Zemax software for design analysis and optimization. Figure 3 shows the lens structure design by the software. For lens optimization, the stop pupil diameter was set to 9 mm in the 13.5 mm diameter Fresnel region. The ratio of the lens focal length to the diameter of the stop pupil diameter ( $F$ -number) of the lens can be calculated using the following equation, Eq. (6):

$$F = \frac{f}{D} \quad (6)$$

where  $f$  is the focal length, and  $D$  is the entrance/stop pupil diameter. The air gap between the two lenses was 0.95 mm, while back focal length (BFL) calculated by the Zemax software was between 10.115 to 10.422 mm for the infinite and 400 mm object distance, respectively. The total track from the entrance pupil to image surface of the design was 16.3 mm. The final design parameters of the lens systems are summarized in Table 2.

Table 2. Design results of lens unit.

Parameters	Value
Wavelength range ( $\mu\text{m}$ ):	8.5-12
Principal wavelength ( $\mu\text{m}$ ):	10
Effective focal length (mm):	10.98
Back focal length for $\infty$ (mm):	10.11
Entrance pupil diameter (mm):	9
F number:	1.29
Field of view (FOV) (degrees):	30
Total track (mm):	16.3

Figure 4(a) shows the ray trace of the lens design by Zemax software at the pupil diameter of 9 mm. The blue, green, red, and yellow lines indicate the incident angles of 0, 7.5, 10.5, and 15°, respectively. From the analysis, it was found that the lens design would have some larger aberration at the angle of 10.5 and 15° as compared to smaller angles. This can be seen more clearly in Fig. 4(b), which shows rather bigger coma aberration of the mentioned angles.

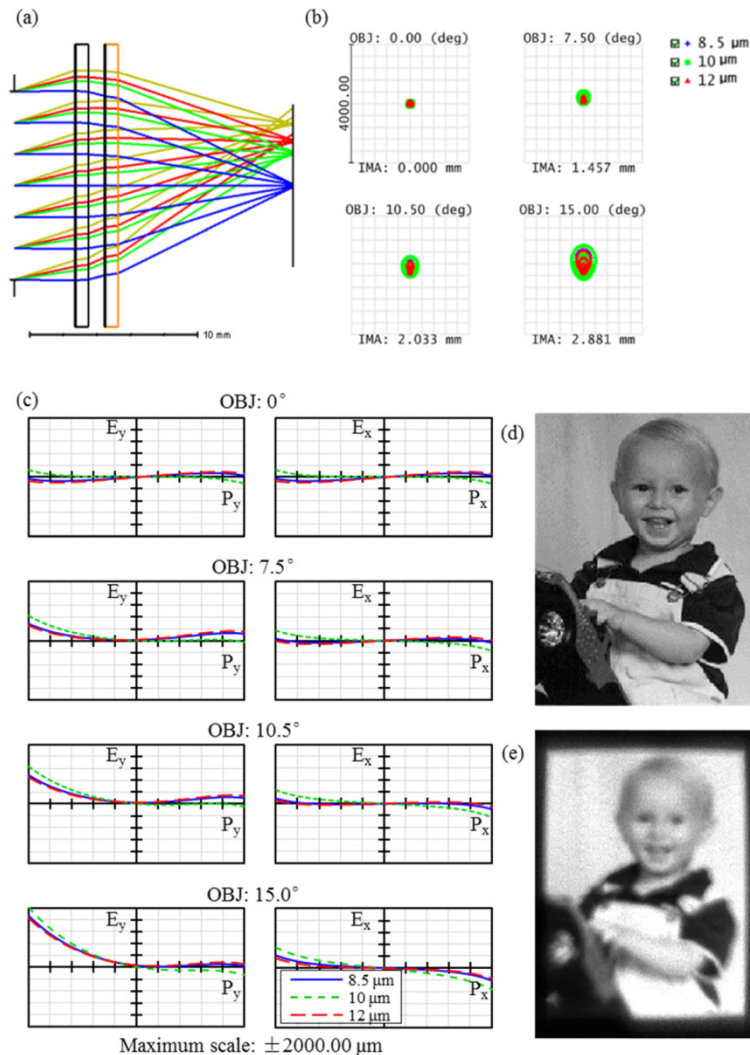


Fig. 4. Zemax lens design data: (a) ray trace of lens system, (b) spot diagram at lens focal point, (c) transverse ray fan plot, (d) original picture of  $288 \times 384$  pixels, and (e) simulated Zemax image of picture (d) of the designed lens.

Figure 4(c) shows tangential ( $P_y$ ) and sagittal ( $P_x$ ) ray aberration as a function of pupil coordinate on different object angles and wavelengths. In the case of an ideal lens system where the paraxial optical model is working, all lines at  $P_y$  and  $P_x$  are zero. However, the ray fan of 8.5, 10, and 12 μm wavelengths start to become off-axis at the incident angle of 7.5° at the  $P_y$  axis. As the angle increases to 10.5° and 15°, the off-axis of the ray aberration increased. Meanwhile, at the  $P_x$  axis, off-axis of the ray aberration is only apparently seen at the angle of 15°.

An image of  $288 \times 384$  pixels in Fig. 4(d) was used to analyze the lens design. From the analyzed image in Fig. 4(e), it shows that the image has some distortion. However, considering other factors, such as the limitation of HDPE thickness that limits the lens design, the image quality can be somewhat compromised.

### 2.3 Mold fabrication

The Fresnel lens structures were machined onto an aluminum mold insert using an ultraprecision diamond lathe, NanoForm X (Ametech Inc., USA), which is equipped with an air bearing spindle. A sharply pointed V-shaped single crystalline diamond tool with an angle of  $60^\circ$  was selected for the cutting process. A constant spindle speed of 2700 rpm was used to roughly cut the surface with a 2.7 mm/min feed rate and a rough cut depth of  $10 \mu\text{m}$ , in which six roughing tool passes were used. The spindle speed and feed rate were unchanged for the semi-finishing cut, but the depth of cut was reduced to  $4 \mu\text{m}$ . The feed rate was then reduced to 0.15 mm/min for finishing. Both the spherical and an aspherical Fresnel molds used the same cutting parameter. A photograph of both mold inserts is shown in Fig. 5. Meanwhile, the surface roughness of the mold was  $4.82 \text{ nm Ra}$ .

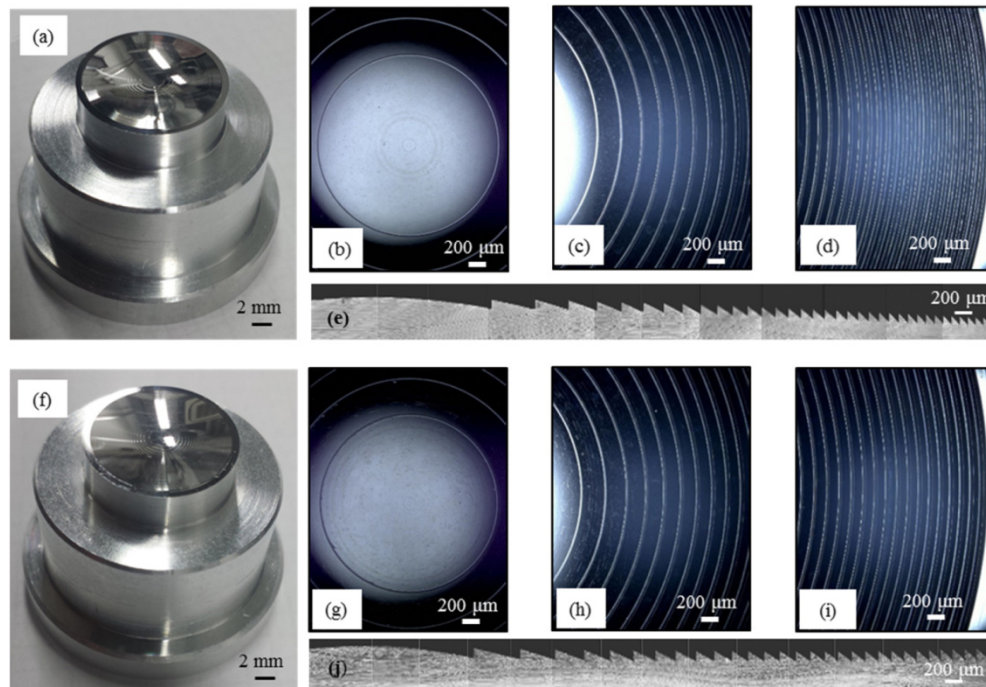


Fig. 5. (a) Photograph of an aluminum mold insert with a spherical Fresnel structure, (b)-(d) microscope images of the spherical Fresnel structure, (e) mold insert cross section of a spherical Fresnel structure obtained by UV curing, (f) photograph of an aluminum mold insert with an aspherical Fresnel structure, (g)-(i) microscope images of an aspherical Fresnel structure, and (j) mold insert cross section of an aspherical Fresnel structure obtained by UV curing.

The sharp ridges of the Fresnel zone caused an error during cross-sectional profile measurement using a laser measuring system. To confirm the Fresnel lens structures machined on the mold, an ultraviolet (UV) curing resin was used to replicate the mold surface, and a cross-section cut was performed on the replicated resin for profile observation using violet laser scanning microscope, VK-9700 (Keyence Co, Japan). It was equipped with a violet laser probe (wavelength 408 nm), which can scan surface three-dimensionally, while the vertical and horizontal resolutions were 1 nm. The cross sections for both lens molds are

provided in Figs. 5(e) and 5(j). From the cross-sectional observation, it shows that the Fresnel structure was accurately fabricated using an ultraprecision diamond lathe with the zone depth of 60  $\mu\text{m}$ .

#### 2.4 Press molding conditions

A press molding machine GMP211 (Toshiba Machine Co. Ltd., Japan) was used for the fabrication of the Si-HDPE hybrid lenses. It is equipped with a transparent silica glass tube chamber that holds the purging nitrogen gas during molding to prevent oxidation of the mold at high temperatures. The molding temperature can rise to 800  $^{\circ}\text{C}$  with a  $\pm 1$   $^{\circ}\text{C}$  tolerance and is monitored by a thermocouple. The pressing force of the machine ranges from 0.2 kN to the maximum of 20 kN with a 0.98 N resolution. The lower mold movement accuracy towards the stationary upper mold is controlled by an AC servomotor with a resolution of 0.1  $\mu\text{m}$ .

In the experiments, two steps of press molding were done as illustrated in Fig. 6. The first step (Step 1) was performing a flat Si-HDPE hybrid substrate using the same method as our previous research [10], as illustrated in Figs. 6(a)-6(c). In this way, the thickness of HDPE can be controlled up to  $\sim 80$   $\mu\text{m}$ . In the second step (Step 2) of press molding, the preformed hybrid substrate is heated above the glass transition ( $T_g$ ) of HDPE and the pressing process will take place. The processes are illustrated in Figs. 6(d)-6(f). Using this two-step method, the air trapping phenomenon that affects the resulting lens surface integrity can be minimized, as found in our previous research [18]. Air pockets were formed at the boundaries between the HDPE pellets and the Si substrate when the HDPE pellets were used in press molding. Thus, the use of flat-shaped HDPE was preferred.

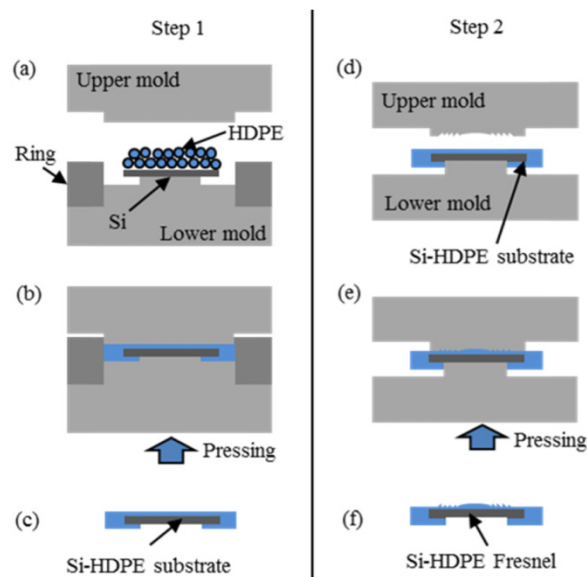


Fig. 6. Press molding process of a Si-HDPE hybrid lens: (a)-(c) hybrid substrate press molding, and (d)-(f) press molding of the Fresnel structure.

In Step 2, three different pressing temperatures were used (125, 128, and 130  $^{\circ}\text{C}$ ). A minimum pressing force of 0.2 kN was used to determine the best pressing temperature. Once the temperature was decided, pressing force was varied from 0.4 to 1.2 kN. The zone depth of the Fresnel lens for different pressing forces was compared to determine the best molding process parameters. In this study, the isothermal molding method was used, where both the mold and molded materials were heated to the same temperature [19]. The molding steps are summarized as follows:

1. A Si-HDPE substrate is placed into the mold cavity. The molding chamber is then closed.
2. The lower mold is raised closer to the stationary upper mold. A 2 mm gap is set between the upper mold and hybrid substrate to enhance the heating process. To prevent mold oxidation during heating, the chamber is purged with nitrogen gas for 20 seconds.
3. Both the molds and specimen are heated by an IR lamp from room temperature to the molding temperature at a heating rate of approximately 0.6 °C/second.
4. The temperature is then maintained for 100 seconds, followed by the pressing until the mold is completely closed. The pressing force is set between 0.4 to 1.2 kN.
5. The pressing force is maintained while nitrogen gas is introduced into the chamber again for cooling at a rate of approximately 0.3 °C/second until the mold temperature was 90 °C. The pressing force is maintained during cooling.
6. Finally, the mold is opened and the molded Si-HDPE hybrid Fresnel lens is demolded from the molds and naturally cooled to room temperature. The time taken for a complete cycle of the press molding process is approximately 420 seconds.

### 2.5 Lens performance characterization

The modulation transfer function (MTF) and effective focal length (EFL) measurements were performed using ImageMaster HR test station (Trioptics Japan Co., Ltd., Japan) at different field angles. The MTF measurement accuracy and repeatability (on-axis and off-axis) of the equipment was  $\pm 0.03$  MTF and  $\pm 0.02$  MTF, respectively. The details of the measurement parameters are listed in Table 3. The result obtained was then compared with the simulated MTF data of Zemax optical design software.

**Table 3. MTF measurement parameters.**

Measurement conditions	Value
Spatial frequency and pitch (lp/mm)	1~10/1
Angle of view (max. image height) / division pitch	15°/5°
Collimator (mm)	50
AF frequency (lp/mm)	5
Total angle of view	30°
Object distance (m)	Infinite
Light source orientation	Sagittal / Tangential
Center wavelength (μm)	10
Wavelength range (μm)	8.2-12.8

Meanwhile, an imaging test was performed in the night mode using the Therm-App (Opgal Optronic Industries Ltd.) IR thermal camera. The camera has a 384 × 288 pixels image sensor with 17 μm pixels pitch. The camera IR spectrum is for long wave IR region (7-14 μm). An Android smartphone was connected to operate the camera. Both formed Fresnel lenses were attached to an aluminum camera housing, which was designed and fabricated with an adjustable mechanism to obtain the required back focal length of the lens during imaging. The camera setup for night mode imaging experiment is shown in Fig. 7, and a human body was selected as the test object. The object was placed at different distances from the camera (400 mm and 2 m) and the image was captured and compared to analyze the performance of the lens.

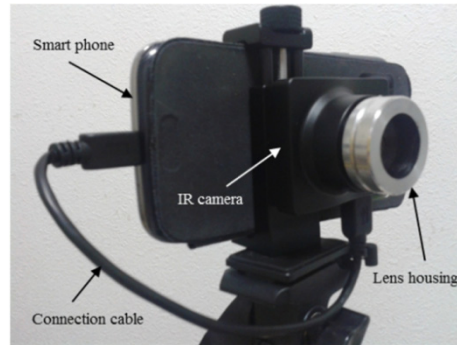


Fig. 7. Camera setup for night imaging performance evaluation.

### 3. Results and discussion

#### 3.1 Fresnel structure transferability

The Si-HDPE Fresnel lens was formed by using press molding under different pressing temperatures. After demolding, the formed lens was replicated by using UV curing process to evaluate the accuracy of press molded microstructures. A cross-section cut was made to the replicated sample from which the Fresnel zone depth was measured. The variations of the zone depth molded at the pressing force of 0.2 kN and pressing temperatures of 125, 128, and 130 °C are illustrated in Fig. 8. Obviously, higher press molding temperature resulted in higher Fresnel zone depth because of the reduction of HDPE viscosity. The zone depth was measured at  $10 \pm 0.309$  and  $16 \pm 0.779$   $\mu\text{m}$  at the temperature of 125 and 128 °C, respectively. As the temperature increased to 130 °C, the zone depth increased to  $20 \pm 0.682$   $\mu\text{m}$ . The result showed that 130 °C might be the suitable temperature to be worked with. The higher the molding temperature, the better the form of accuracy [12].

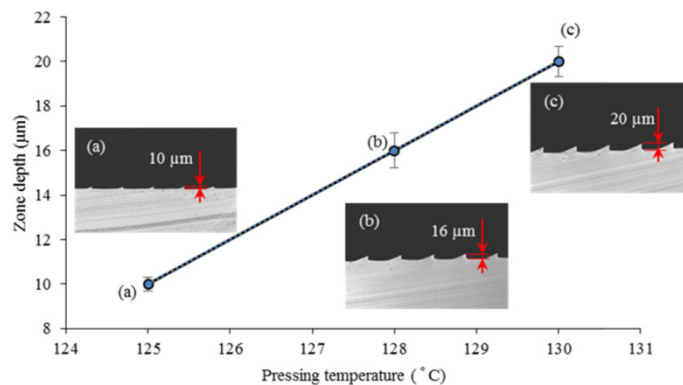


Fig. 8. Zone depth change of the Fresnel structure for different temperatures under the pressing force of 0.2 kN.

Under the 130 °C pressing temperature, a series of press molding experiments was done with the pressing force varying from 0.6 to 1.2 kN. The microscope images of the formed Fresnel lenses are illustrated in Fig. 9, where the images were divided into three sections: top views of center and outer region, and cross-section view of the lens. In Figs. 9(a)-9(d), it was found that the center area of the lens was incompletely formed for all pressing forces and an unformed area was observed. Also, rounded Fresnel edges were noticed at the outer area, as shown in Figs. 9(e) and 9(f), when it was formed at the pressing force of 0.6 and 0.8 kN. This phenomenon might be due to insufficient pressing force and polymer recovery [20]. The

increase of pressing force to 1.0 and 1.2 kN improved the lens structures, and rounded edges were eliminated, as shown in Figs. 9(g) and 9(h).

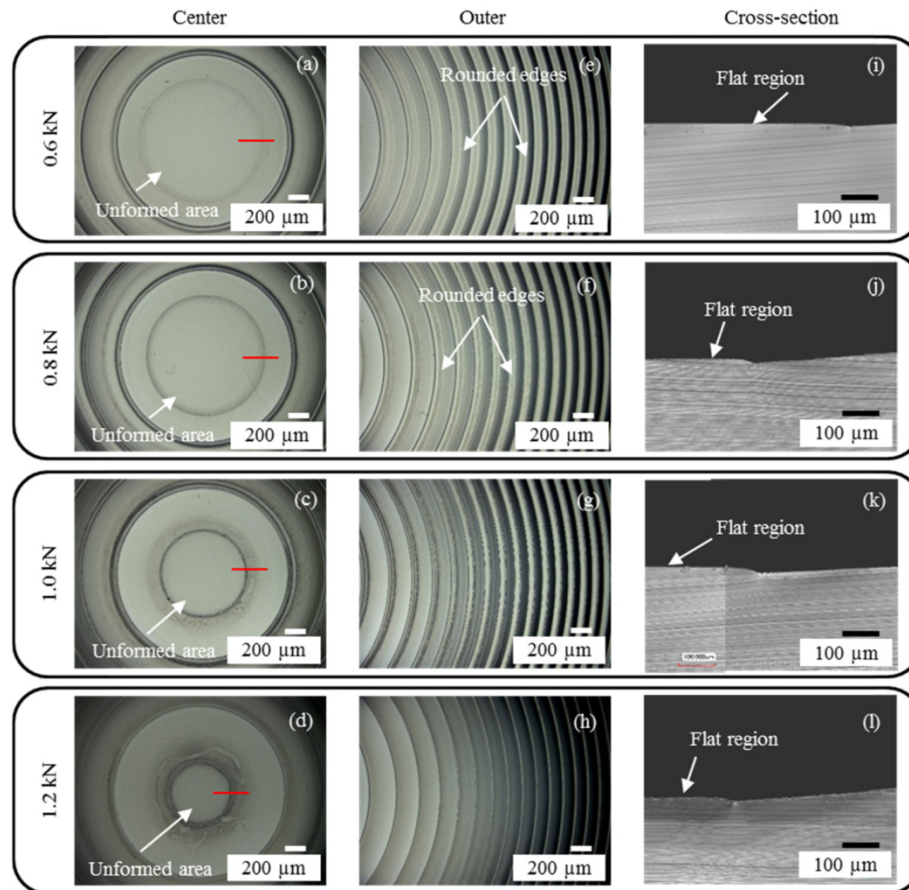


Fig. 9. Microscope images of formed Fresnel lens under different pressing forces at a temperature of 130 °C.

For further investigation, the cross section of the center area was made and illustrated in Figs. 9(i)-9(l). From these cross-section observations, it was found that some of the center areas remained flat for all pressing forces. As expected, the flat area decreased gradually when increasing the pressing force. However, the increase of pressing forces up to 1.2 kN did not eliminate the flat area. This might be due to insufficient pressing temperature.

To evaluate the dimensional accuracy of the press molded lens under 130 °C, a cross-section measurement of zone depth was done, and the results are plotted in Fig. 10. The zone depth was measured at  $22 \pm 0.339$  and  $46 \pm 0.141$  μm when it formed at a pressing force of 0.6 and 0.8 kN respectively. As the pressing force increased to 1.0 and 1.2 kN, the zone depth increased to  $53 \pm 0.230$  and  $54 \pm 0.304$  μm. Although the pressing force increased, the target zone depth of 60 μm was not achieved. From this outcome, the pressing temperature of 130 °C is unsuitable for achieving form accuracy.

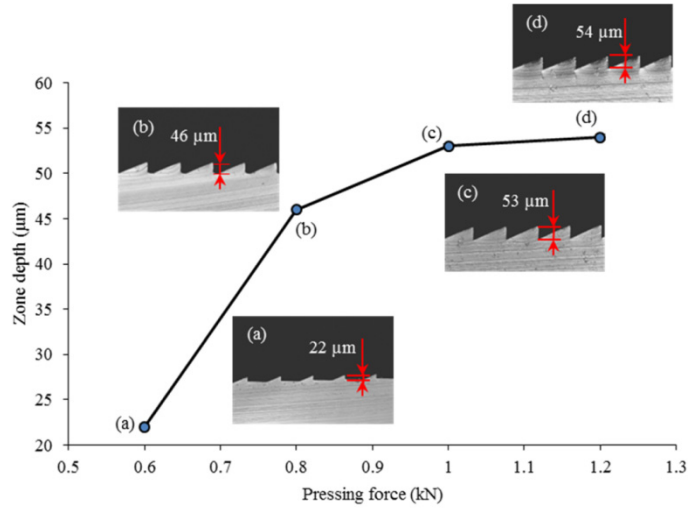


Fig. 10. Zone height of the Fresnel under different pressing forces at a temperature of 130 °C.

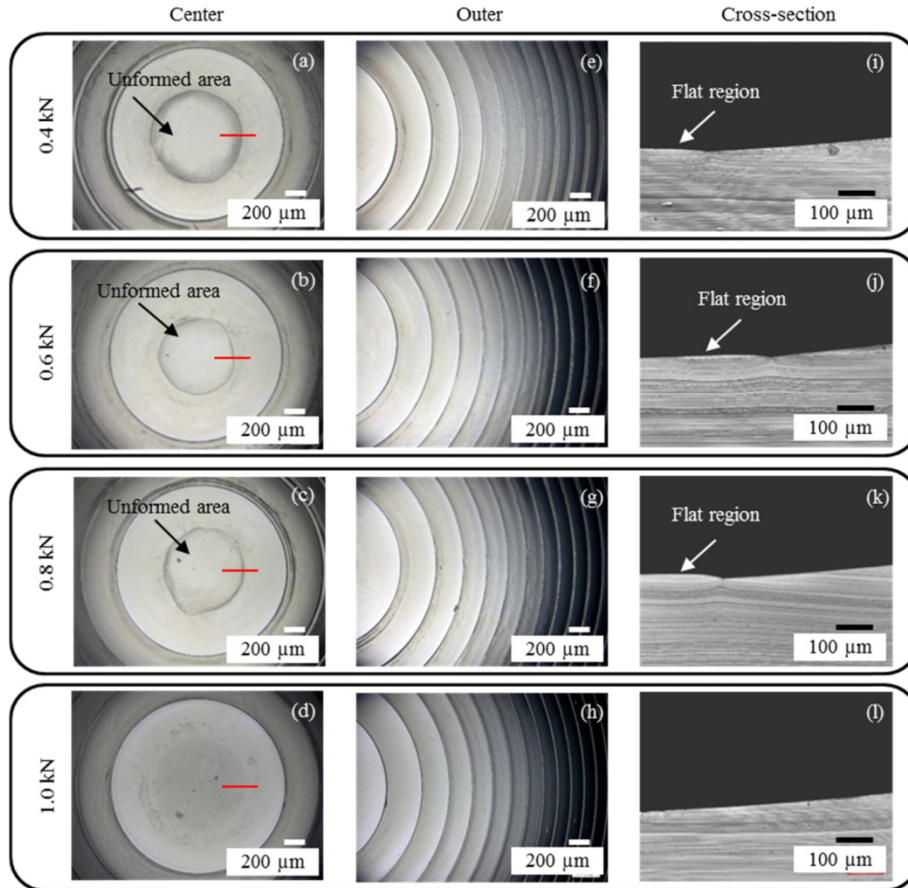


Fig. 11. Microscope images of formed Fresnel lens under different pressing forces at a temperature of 131 °C.

Next, the pressing temperature was slightly increased to 131 °C, and a press molding experiment was performed. The temperature (131 °C) was selected as the use of higher temperature resulted in higher polymer shrinkage, thus the form accuracy will be affected [21]. Figure 11 shows microscope images of the Fresnel formed at the pressing forces of 0.4 to 1.0 kN. The rounded edges were significantly reduced for all pressing forces compared with previous experiments (see Fig. 9). This phenomenon is due to the low viscosity of the polymer, which makes polymer flow smoothly inside the cavity [21]. Meanwhile, an unformed area persisted at a pressing force of 0.4 kN, as shown in Fig. 11(a). The unformed area was reduced by gradually increasing the pressing force to 0.6 and 0.8 kN, as shown in Figs. 11(b) and 11(c). The unformed area was completely eliminated when 1.0 kN of pressing force was used, as shown in Fig. 11(d). This was also confirmed by the cross-section area observation in Fig. 11(l), where the Fresnel curvature was obtained completely and the flat area was eliminated.

Figure 12 shows the change of zone depth of the Fresnel lens formed at the pressing temperature of 131 °C. The zone depth was  $57 \pm 0.158$  and  $57.6 \pm 0.083$   $\mu\text{m}$  when the pressing force was 0.4 and 0.6 kN. As the force increased to 0.8 kN, the zone depth increased to  $58.3 \pm 0.070$   $\mu\text{m}$ . The Fresnel lens was accurately formed at the pressing force of 1.0 kN, and the zone depth of  $60 \pm 0.083$   $\mu\text{m}$  was obtained precisely. These results clearly show that the form accuracy depends on the pressing temperature, similar to hot embossing [12]. Figure 13(a) shows the cross-sectional profile of the formed Fresnel. It can be seen that the lateral structures of the lens were also formed precisely. Based on these results, it is estimated that the press molding temperature of 131 °C and the pressing force of 1.0 kN were the optimal molding parameters for the Fresnel lens in this work. Under such conditions, the surface roughness of 6.78 nm Ra was achieved on the molded lens. Figure 13(b) is a photograph of a formed Si-HDPE hybrid Fresnel lens and a coin for comparison of size.

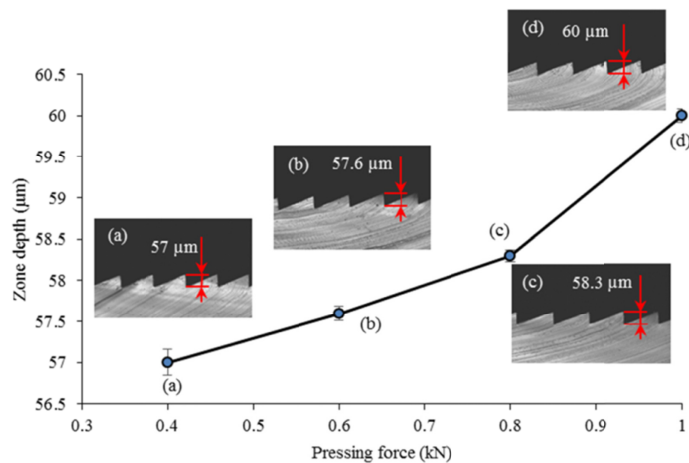


Fig. 12. Zone height of the Fresnel under different pressing forces at a temperature of 131 °C.

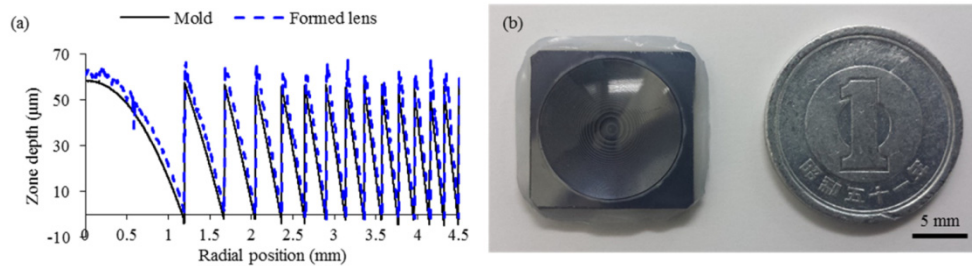


Fig. 13. (a) Cross-sectional profile of lens geometry, (b) a press molded Si-HDPE hybrid Fresnel lens and a Japanese coin.

To examine the interface between Si and HDPE after press molding, a press molded Si-HDPE Fresnel lens cross-section was observed by a scanning electron microscope (SEM). Figure 14 shows the cross-sectional SEM images of the sample. No gap was seen between the two materials in which it demonstrates that the HDPE was bonded directly to Si during press molding by crosslinking binding [10].

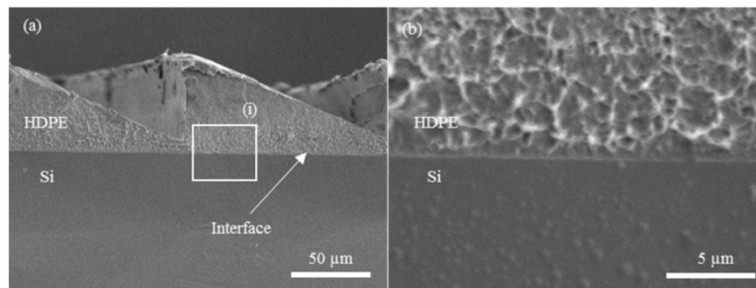


Fig. 14. (a) Cross-sectional SEM images of a Si-HDPE Fresnel lens; (b) magnified view of rectangle (i) showing the interface.

### 3.2 Lens optical performance

MTF shows the modulation (contrast) response capabilities of a lens system for each spatial frequency, and different tangential/sagittal angle. In this study, the MTF was measured at a wavelength of 10 μm and the field angle varied from 0 to 15°, with an angle pitch of 5°. The experimental MTF data was compared with the theoretical geometric MTF obtained by Zemax, and is illustrated in Fig. 15. In the figure, there is a good agreement between the experimental data and the theoretical MTF. The experimental curve stands below the simulated MTF at the field angle of 0° as shown in Fig. 15 (a), resulting in lower image contrast. The difference of the measured and the simulated MTF is due to errors caused by poor line image density or line spread function (LSF) during MTF measurement. In some cases LSF is barely obtained because of the darkness of the image, thus autofocusing was used to obtain reliable measurement data.

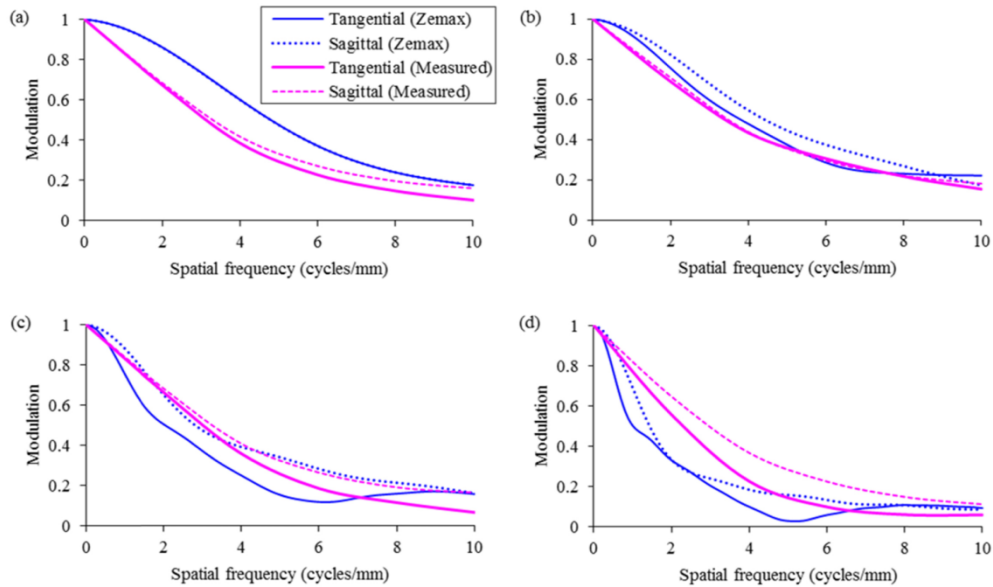


Fig. 15. Comparison of geometric MTF calculated by Zemax and measured results for different field angles: (a)  $\theta = 0^\circ$ , (b)  $\theta = 5^\circ$ , (c)  $\theta = 10^\circ$ , and (d)  $\theta = 15^\circ$ .

As the field angle increased to  $5^\circ$  and  $10^\circ$  as shown in Figs. 15(b) and 15(c) respectively, the frequency dependence of tangential and sagittal from the measured and simulated data are almost the same. However, a higher contrast was noticed at the measured tangential frequency of  $10^\circ$  field angle at a lower frequency. The measured MTF continued to show better performance at a lower frequency as illustrated in Fig. 15(d) as the field angle increased to  $15^\circ$ , and continued on the same pattern with the simulated MTF as the frequency increased. The slight differences between the simulated and the measured MTF curve were also due to the differences of the light passing through the diffractive surfaces of the lenses. In the overall performance for all field angles, the MTF curve stands 0.1 above the modulation. This means that our fabricated lens results in relatively low contrast images.

Meanwhile, as shown in Fig. 16(a), the measured distortion percentage shows a similar pattern as the results simulated by Zemax with an approximately 1% difference. A series of EFL measurements at the wavelength of  $10 \mu\text{m}$  was also done and illustrated in Fig. 16(b), where the average measured focal length was 9.6 mm. Although there is a difference in the measured results, all of the measured focal lengths are in the tolerance of  $\pm 1.5 \text{ mm}$  with respect to the designed focal length (10.982 mm).

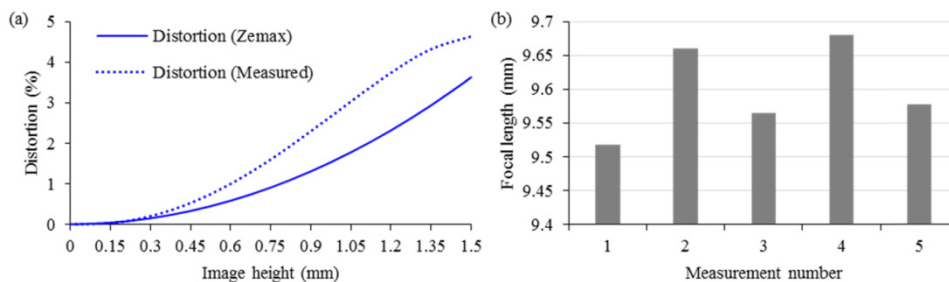


Fig. 16. (a) Zemax-simulated and measured image distortion, (b) focal length measurement results at a wavelength of  $10 \mu\text{m}$ .

### 3.3 Night mode imaging

The press molded lenses were assembled with the lens housing and attached to the IR camera for night mode imaging. The white-hot imaging mode was selected for the camera setting. Night vision images captured by using a double Si-HDPE hybrid Fresnel lens are shown in Fig. 17, which was captured at the distances of 400 mm and 2 m. For comparison, visible light images were also listed in the same figure. After pixel correction, at a shorter imaging distance (400 mm), an acceptable image quality was obtained where details of the object could be seen. At a longer distance (2 m), the object shape was still identifiable even though it lost some image sharpness because of the chromatic aberration of the lens systems. As seen from the MTF measurement result, the contrast of the image is low, resulting in a dark image.



Fig. 17. Visible light and night vision images at different distances; (a)-(b) 400 mm and (c)-(d) 2 m, and rectangle (i) showing image aberration.

Meanwhile, image distortion is not identifiable from the captured image due to low contrast of the images, even though the measured distortion showed slightly higher values than the Zemax estimation, as discussed earlier in Section 3.2. Chromatic aberration was also detected in the IR image, as shown in Fig. 17(d) in rectangle (i), which resulted in blurred images due to stray light from the lens system. The stray light might be caused by light scattering at the edges and wall of the Fresnel structure, as well as light reflection from the Si substrate [22]. Figure 18 shows the stray light generation in the lens system. Meanwhile, the difference between lens design wavelength (8.5-12  $\mu\text{m}$ ) and image sensor sensitivity wavelength (7-14  $\mu\text{m}$ ) also degraded the image quality and resulted in the blurred image.

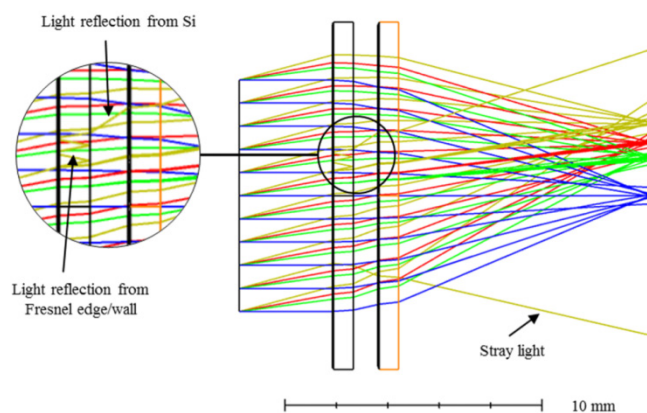


Fig. 18. Schematic diagram of stray light formation from the lens system.

To show the ability of the developed Si-HDPE hybrid lens to work with other IR lens materials to further improve its imaging quality, imaging trials were done by combining a

spherical hybrid Fresnel lens (Lens 1) and a Ge convex-concave lens. The lens systems schematic diagram is illustrated in Fig. 19(a). The captured images of using this lens combination are shown in Figs. 19(b) and 19(c). The chromatic aberration is minimized as shown in Fig. 19(c) in rectangle (i), which might be due to reduced stray light, and better IR transmittance of Ge. Clearer and sharper images are obtained compared with the double Si-HDPE hybrid lenses, which can be seen from Fig. 20. From the figure, it indicates that higher gray value is recorded when a combination of hybrid Fresnel and Ge convex-concave lens was used, compared with the double hybrid Fresnel. This demonstrates that the use of the developed hybrid lens in combination with other IR lens material is possible, which greatly improves the imaging quality of the developed lens system for higher-precision applications.

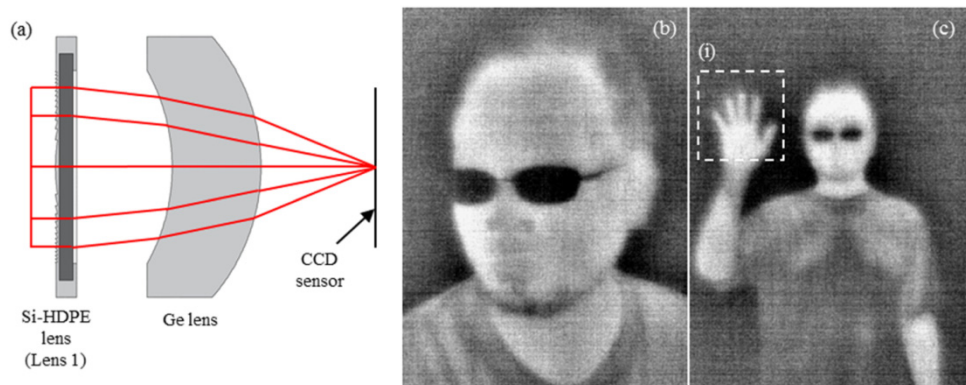


Fig. 19. (a) Schematic diagram of combining a Si-HDPE hybrid lens and germanium lens, (b) night vision images captured by combining a Si-HDPE hybrid lens and a germanium lens at different distances; (b) 400 mm and (c) 2 m, and rectangle (i) showing image aberration.

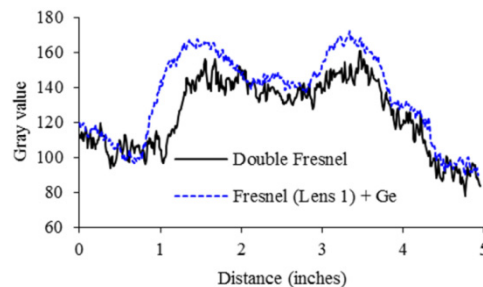


Fig. 20. Image sharpness evaluation between double Si-HDPE hybrid Fresnel and a combination of a spherical Si-HDPE hybrid Fresnel (Lens 1) + Ge.

### 3.4 Thermography mode imaging

A thermography imaging trial has also been done by using a double Si-HDPE hybrid Fresnel lens are shown in Fig. 21. The captured image showed the lens systems are also capable of being used in thermography application. There is no significant difference in the image quality between standard Ge lens systems (Therm-App 19 mm lens) and Si-HDPE hybrid Fresnel. The temperature distribution of the object can be recognized and measured, although the temperature value and accuracy need to be calibrated to realize the use of hybrid lenses for thermography applications.

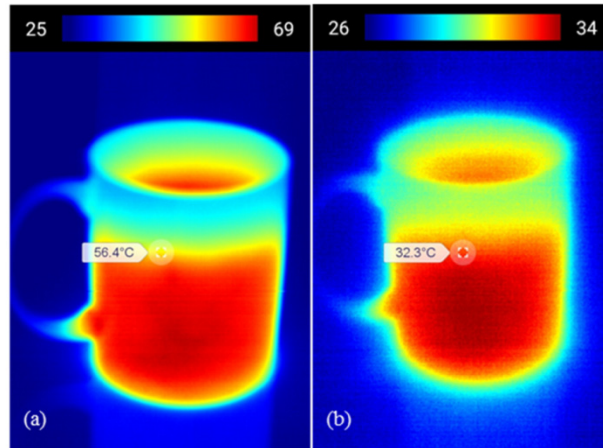


Fig. 21. Thermography images of different lens systems: (a) standard germanium lens and (b) uncalibrated double Si-HDPE hybrid Fresnel.

#### 4. Conclusion

A Si-HDPE hybrid Fresnel lens system for infrared imaging applications has been designed and fabricated. The form accuracy and optical capabilities of the fabricated lenses were evaluated. The following conclusions were obtained:

1. Fresnel structures were precisely formed on an 80  $\mu\text{m}$ -thick layer of HDPE to form an ultrathin Si-HDPE hybrid infrared lens, which has a total thickness of  $\sim 800$   $\mu\text{m}$ . Such a thin IR lens has never been reported in the literature.
2. The lens form accuracy depends on pressing force and temperature. Increasing both parameters improves the Fresnel shape transferability. A molding temperature of 131  $^{\circ}\text{C}$  and a pressing force of 1.0 kN were the optimal molding parameters for the Fresnel lens under the present experimental conditions.
3. The measured modulation transfer function of the fabricated lens system showed similar results to the simulated data by the Zemax optical design software.
4. The fabricated hybrid lens system produced satisfactory image quality in the night mode, with a slightly lower image contrast than that of Ge lenses.
5. The ability of the lens systems in thermography imaging was also demonstrated. The temperature distribution was properly detected by the developed lenses.
6. A combination of a Si-HDPE hybrid lens and a concave-convex Ge lens produced a higher quality image than the double Si-HDPE hybrid lens system, which provided the possibility of using the fabricated hybrid lens in combination with other IR material lenses for high-precision infrared systems.

This paper demonstrated the possibility of a cost-effective method for fabricating compact and high-performance IR optical components for night vision systems. These lenses might have the potential for applications in future infrared optical technologies for rescue, night surveillance, night driving assistance, as well as thermography.

#### Funding

Keio University KLL Research Grant (000002) for Ph.D. Program for 2016 Academic Year.

## Acknowledgments

The authors would like to thank Mr. Mao Mukaida for his assistance in diamond turning of the molds used in this study. Thanks are extended to Mitsubishi Chemical Corporation, Global Wafers Japan Co., Ltd., and Trioptics Japan Co., Ltd., for providing HDPE, Si samples, and technical data, as well as optical measuring services.